PCCP

Formation of Methylglyoxal ($CH_3C(O)CHO$) in Interstellar Analog Ices – A Key Intermediate in Cellular Metabolism

Journal:	*Physical Chemistry Chemical Physics*
Manuscript ID	CP-ART-07-2024-002779.R1
Article Type:	Paper
Date Submitted by the Author:	21-Aug-2024
Complete List of Authors:	Wang, Jia; University of Hawai'i at Manoa, Department of Chemistry; University of Hawai'i at Manoa, W. M. Keck Research Laboratory in Astrochemistry Marks, Joshua ; University of Hawai'i at Manoa, Department of Chemistry; University of Hawai'i at Manoa, W. M. Keck Research Laboratory in Astrochemistry Batrakova, Evgeniya; Samara National Research University Tuchin, Sergey; Samara National Research University Antonov, Ivan; Samara National Research University Kaiser, Ralf; University of Hawaii,

Formation of Methylglyoxal ($CH_3C(O)CHO$) in Interstellar Analog Ices – A Key Intermediate in Cellular Metabolism

Jia Wang,[1,2] Joshua H. Marks,[1,2] Evgenia A. Batrakova,[3] Sergey O. Tuchin,[3] Ivan O. Antonov,[3*] Ralf I. Kaiser[1,2*]

[1] W. M. Keck Research Laboratory in Astrochemistry, University of Hawaii at Manoa, Honolulu, HI 96822, USA

[2] Department of Chemistry, University of Hawaii at Manoa, Honolulu, HI 96822, USA

[3] Samara National Research University, Samara 443086, Russia

[*]Corresponding Authors:

Ivan Antonov, pfizeke@gmail.com

Ralf I. Kaiser, ralfk@hawaii.edu

Abstract

Ketoaldehydes are key intermediates in biochemical processes including carbohydrate, lipid, and amino acid metabolism. Despite their crucial role in the interstellar synthesis of essential biomolecules necessary for the *Origins of Life*, their formation mechanisms have largely remained elusive. Here, we report the first bottom-up formation of methylglyoxal ($CH_3C(O)CHO$) — the simplest ketoaldehyde — through the barrierless recombination of the formyl ($H\dot{C}O$) radical with the acetyl ($CH_3\dot{C}O$) radical in low-temperature interstellar ice analogs upon exposure to energetic irradiation as proxies of galactic cosmic rays. Utilizing vacuum ultraviolet photoionization reflectron time-of-flight mass spectrometry and isotopic substitution studies, methylglyoxal and its enol tautomer 2-hydroxypropenone ($CH_3C(OH)CO$) were identified in the gas phase during the temperature-programmed desorption of irradiated carbon monoxide–acetaldehyde ($CO–CH_3CHO$) ices, suggesting their potential as promising candidates for future astronomical searches. Once synthesized in cold molecular clouds, methylglyoxal can serve as a key precursor to sugars, sugar acids, and amino acids. Furthermore, this work provides the first experimental evidence for tautomerization of a ketoaldehyde in interstellar ice analogs, advancing our

fundamental knowledge of how ketoaldehydes and their enol tautomers can be synthesized in deep space.

Introduction

Since the first preparation of the simplest ketoaldehyde — methylglyoxal ($CH_3C(O)CHO$, **1**) — by von Pechmann more than 130 years ago,[1] **1** has attracted considerable attention as a crucial intermediate in biochemical processes from the astrochemistry,[2-6] astrobiology,[7,8] and physical organic chemistry communities.[9,10] Ubiquitous in all cells, **1** is produced as a by-product of carbohydrate, lipid, and amino acid metabolism[11,12] and plays a central role in the methylglyoxal pathway, an alternative to glycolysis.[13] In the methylglyoxal pathway, glucose ($C_6H_{12}O_6$, **2**) is converted into pyruvate without the generation of adenosine triphosphate (ATP).[14] After its formation via glycerol kinase and glycerol 3-phosphate dehydrogenase, dihydroxyacetone phosphate ($C_3H_7O_6P$, **3**) is converted to **1** by methylglyoxal synthase (Fig. 1).[15] Subsequently, lactaldehyde ($CH_3CH(OH)CHO$, **4**) can be synthesized from **1** by methylglyoxal reductase and then converted to lactic acid ($CH_3CH(OH)COOH$, **5**) via aldehyde dehydrogenase.[16] Through lactate dehydrogenase, **5** further leads to the formation of pyruvic acid ($CH_3COCOOH$, **6**),[15] which is a critical molecule linked to the tricarboxylic acid (TCA) cycle.[17,18]

In prebiotic chemistry, **1** can serve as a fundamental precursor for vital biomolecules such as amino acids, sugars, and sugar acids (Fig. 1). Oxidation of **1** results in the formation of **6**, a molecular building block of amino acids. Upon exposure to ionizing radiation, **1** may react with ammonia (NH_3) to form the proteinogenic amino acid alanine ($NH_2CH(CH_3)COOH$, **7**), ultimately producing complex amino acids and peptides. Triggered by energetic radiation, **1** can react with water (H_2O) to yield dihydroxyacetone ($HOCH_2C(O)CH_2OH$, **8**) and the simplest sugar molecule glyceraldehyde ($HOCH_2CH(OH)CHO$, **9**), contributing to the synthesis of complex sugars. Reduction of **1** leads to the formation of **4**, which can then be oxidized to **5** eventually contributing to the formation of sugar acids such as glyceric acid ($HOCH_2CH(OH)COOH$, **10**).[19] Under interstellar conditions, interstellar ices composed of simple molecules such as water, carbon monoxide (CO, **11**), carbon dioxide (CO_2), methanol (CH_3OH, **12**), ammonia, and methane (CH_4) condensed on nanoparticles at typically 10 K are subjected to the ionizing radiation from galactic cosmic rays (GCRs) or ultraviolet (UV) photons; this exposure could result in the formation of biologically relevant molecules including **1**.[2,18,20,21] Although **1** has not yet been identified in the

interstellar medium (ISM),[22] laboratory simulation experiments have detected **1** in the simulated pre-cometary organic residues following the vacuum ultraviolet (VUV) irradiation of ices composed of **12** and water,[3] suggesting that **1** can form in the interstellar ices. Additionally, astrochemical models suggested a formation route of **1** on the grain surface via barrierless recombination of the formyl (HĊO, **13**) and acetyl ($CH_3\dot{C}O$, **14**) radicals,[2,6] predicting a relatively high abundance of 2×10^{-3} for **1** with respect to methanol.[6] However, experimental mechanistic evidence on its formation under interstellar conditions on ice-coated nanoparticles at 10 K has remained elusive. Unraveling the formation pathways of **1** is therefore of fundamental importance for advancing our knowledge of the molecular mass-growth processes of astrobiologically relevant molecules in deep space and their role in contemporary cellular metabolisms.

Here, we present the first bottom-up formation of the simplest ketoaldehyde **1** in low-temperature interstellar ice analogs upon exposure to energetic irradiation as proxies of GCRs.[21,23-28] This was accomplished in irradiated carbon monoxide–acetaldehyde (CO–CH_3CHO, **11**–**15**) ice mixtures and observing the barrierless recombination of the formyl (**13**) radical with the acetyl (**14**) radical (Figs. 1 and 2). Radicals **13** and **14** were identified in irradiated ices via Fourier-transform infrared spectroscopy (FTIR). Utilizing isomer-selective VUV photoionization reflectron time-of-flight mass spectrometry (PI-ReToF-MS) and isotopic substitution studies, **1** and its enol tautomer 2-hydroxypropenone ($CH_3C(OH)CO$, **16**) were identified in the gas phase during the temperature-programmed desorption (TPD) of irradiated ices based on their adiabatic ionization energies (IEs). This finding reveals key formation routes of crucial biorelevant organics — ketoaldehydes — as well as their enol tautomers in interstellar environment. In interstellar ices, **11** has been detected at fractions of up to 55% with respect to water toward IRAS 08375–4109;[29] **15** has been tentatively identified at levels of up to a few percent with respect to water toward the protostar W33A.[30] Therefore, **1** and **16** could have been formed in interstellar ices containing **11** and **15** via the formation pathways demonstrated here. The chemistry of enols in the ISM has gained increasing attention with the recent discovery of (*Z*)-1,2-ethenediol (HOCHCHOH) toward the G+0.693−0.027 molecular cloud.[31] Once synthesized in cold molecular clouds, **1** can be integrated into planetesimals and eventually delivered to the early Earth via comets and meteorites, thus providing an exogenous source for the synthesis of vital biomolecules critically linked to the *Origins of Life*.

Experimental and Computational

All experiments were conducted in an ultrahigh vacuum chamber maintained at pressures of 5 × 10^{-11} Torr using magnetically levitated turbomolecular pumps and a dry scroll pump.[32] The experimental samples consist of carbon monoxide (CO, 99.99%, Sigma Aldrich), isotopically labeled carbon monoxide ($C^{18}O$, Sigma-Aldrich, 95 atom % ^{18}O), acetaldehyde (CH_3CHO, Sigma Aldrich, anhydrous, ≥99.5% purity), and isotopically labeled acetaldehyde (CD_3CDO, Sigma Aldrich, ≥ 99 atom % D). The acetaldehyde sample was stored in a glass vial connected to a high vacuum chamber at pressures of several 10^{-8} Torr after several freeze-thaw cycles to remove residual atmospheric gases. Carbon monoxide was premixed with acetaldehyde vapor to prepare a gas mixture of 50 Torr carbon monoxide and 20 Torr acetaldehyde. During deposition, the gas mixture was introduced into the main chamber at 4 × 10^{-8} Torr through a glass capillary array and directed onto a polished silver substrate. The substrate was cooled to 5 K using a two-stage closed-cycle helium refrigerator that can be freely rotated and translated vertically.[32] Laser interferometry was used to measure the ice thickness from the interference fringes.[33] Based on the average refractive index (n) of 1.28 ± 0.03 between the refractive index of carbon monoxide ice (n = 1.25 ± 0.03)[34] and that of acetaldehyde (n = 1.303),[35] the ice thickness was determined to be 750 ± 30 nm (Table S1). A Fourier transform infrared (FTIR) spectrometer (Thermo Electron, Nicolet 6700) was utilized to monitor the deposited ices *in situ* in the range of 500 − 6000 cm^{-1} with a spectral resolution of 4 cm^{-1}. Considering the density of carbon monoxide (0.80 ± 0.01 g cm^{-3})[34] and acetaldehyde (0.787 g cm^{-3}),[35] the ice composition of carbon monoxide to acetaldehyde was determined to be 1.2 ± 0.5:1. This was done by integrating the infrared absorptions of carbon monoxide at 2136 cm^{-1} (ν_1, 1.12 × 10^{-17} cm $molecule^{-1}$) and 4249 cm^{-1} ($2\nu_1$,1.04 × 10^{-19} cm $molecule^{-1}$),[34] and of acetaldehyde at 1349 cm^{-1} (ν_7, 1.1 × 10^{-18} cm $molecule^{-1}$) and 1122 cm^{-1} (ν_8, 6.6 × 10^{-19} cm $molecule^{-1}$),[36] and the FTIR spectra of pure acetaldehyde ices with known thickness.[37]

After deposition, the ice mixtures were exposed to 5 keV electron irradiation (SPECS, EQ PU-22) with low dose (24 nA, 5 minutes) or high dose (37 nA, 30 minutes) at an incidence angle of 70°. Monte Carlo simulations performed in the CASINO software suite[38] showed that these irradiation conditions correspond to doses of up to 1.35 ± 0.19 eV $molecule^{-1}$ for carbon monoxide and 2.65 ± 0.37 eV $molecule^{-1}$ for acetaldehyde; these conditions simulate secondary electrons

produced in the track of GCRs in cold molecular clouds aged (6 ± 2) × 10^6 years.[39] The average penetration depth of the electrons was determined to be 380 ± 40 nm. Furthermore, 99% of the electron energy was deposited within the top depth of 660 ± 50 nm, which is less than the ice thickness of 750 ± 30 nm, preventing interaction between the electrons and the substrate. The FTIR spectra were collected to monitor the chemical changes in ices during irradiation. After irradiation, temperature-programmed desorption (TPD) was performed by heating the ice from 5 K to 320 K at a rate of 0.5 K minute^{-1}. Sublimating molecules were photoionized into the gas phase by pulsed VUV photons with a repetition rate of 30 Hz. The resulting ions were detected by a dual microchannel plate (MCP) using reflectron time-of-flight mass spectrometry (ReToF-MS, Jordan TOF Products). Multiple VUV photons at 11.10 eV, 9.87 eV, 9.39 eV, 8.77 eV, and 7.60 eV were generated via resonant four-wave mixing using two dye lasers (Sirah, Cobra-Stretch) and two Nd: YAG lasers (Spectra-Physics, Quanta Ray Pro 250-30 and 270-30). Detailed VUV generation parameters are listed in Table S2. The VUV light was separated from other laser beams using a biconvex lithium fluoride lens in an off-axis geometry, passing 2.0 ± 0.5 mm above the ice surface to ionize sublimating molecules. Ion signals were amplified with a preamplifier (Ortec 9305) and recorded with a multichannel scaler (FAST ComTec, MCS6A). For each mass spectrum, the accumulation time of the ion signals was 2 minutes (3600 sweeps) with an arrival time accuracy of 3.2 ns. An additional blank experiment was performed without irradiation at 11.10 eV for CO–CH_3CHO ice, and no sublimation event was observed at m/z = 72.

The CBS–QB3 composite approach was used to perform calculations and obtain accurate values for the energies of the cationic and neutral states of each species. Molecular parameters and energies can be obtained with an accuracy of 0.01–0.02 Å for bond lengths, 1–2° for bond angles, and 4–8 kJ mol^{-1} for relative energies. The GAUSSIAN 09 package was employed for all *ab initio* electronic structure calculations.[40] Five backbone isomers of $C_3H_4O_2$ products were identified, differing in the position of the hydroxyl, carbonyl, and methyl groups, namely methylglyoxal (**1**), 2-hydroxypropenone (**16**), propanedial (**18**), 2-hydroxypropenal (**19**), and 3-hydroxypropenal (**20**). To obtain accurate ionization energies for each isomer, all possible isomers formed by rotation around specific C−O or C−C single bond (referred to as conformers) were considered. A computer software was developed to accomplish this task of automatically preparing GAUSSIAN 09 input files for each conformer. The Python source code of the program is available in the Supplementary Source code. Methylglyoxal (**1**) exists in two stable conformations, (*anti*)-

methylglyoxal (**1a**) and (*syn*)-methylglyoxal (**1b**) with respect to two carbonyl groups (C=O). The most energetically favorable isomer is (*anti*)-methylglyoxal (**1a**). The calculated conformer energies relative to **1a** and the adiabatic ionization energies (IEs) are shown in Fig. 2. The IE of **1a** was experimentally determined to be 9.60 ± 0.06 eV,[41] which agrees well with our calculated value (9.60 eV). The Cartesian geometries, vibrational frequencies and infrared intensities, and dipole moments of the computed structures are provided in Tables S3–S8.

Results and Discussion

Infrared Spectroscopy

Infrared spectra of carbon monoxide–acetaldehyde ices were collected at 5 K before, during, and after the irradiation (Figs. S1–S5). Detailed assignments of the FTIR spectra are compiled in Tables S9–S13. After the gas deposition, all absorptions can be attributed to the fundamentals and combination modes of the reactants, such as the prominent absorptions of the CO stretching at 2136 cm^{-1} for **11**[34] and the stretching mode of the carbonyl moiety at 1722 cm^{-1} for **15**.[42] During and after the irradiation, several new absorption features emerged (Figs. S1–S2). Carbon dioxide and methane were detected through the C=O stretching mode (CO_2, ν_3) at 2342 cm^{-1} and the deformation mode (CH_4, ν_4) at 1304 cm^{-1}.[34] The absorption bands at 3343 cm^{-1} and 2941 cm^{-1} correspond to the O–H stretching mode and C–H stretching mode, respectively. The absorptions at 1852 cm^{-1}, 1841 cm^{-1}, and 1571 cm^{-1} are linked to **13** (HĊO, ν_3), **14** (CH_3ĊO, ν_3) and hydroxycarbonyl (HOĊO, ν_2), and the vinoxy (ĊH_2CHO, **17**, ν_4) radicals, respectively (Figs. 3, and S1–S2, Tables S9–S10).[43-45] These radicals were further confirmed in irradiated CO–CD_3CDO ices (Figs. 3, and S3–S4) shifted to 1851 cm^{-1} for **14-**d_3 (CD_3ĊO, ν_3), 1794 cm^{-1} for **13-**d_1 (DĊO, ν_3), 1786 cm^{-1} for hydroxycarbonyl-d_1 (DOĊO, ν_2), and 1513 cm^{-1} for **17-**d_3 (ĊD_2CDO, ν_4).[43,44] The temporal evolutions of these radicals during irradiation are provided in Fig. S6. Additionally, the absorptions at 2498 cm^{-1} and 1578 cm^{-1} in irradiated CO–CD_3CDO ices are linked to the O–D stretching and the C=O and/or C=O stretching bands of the formed products. Niki et al. measured IR absorptions of **1** at 2828, 1733, and 1368 cm^{-1} with gaseous sample pressures in the torr range.[46,47] The absorption features of propanedial ($HCOCH_2CHO$, **18**) were observed at 2832, 1683, 1391, 1118, and 907 cm^{-1} in the liquid phase.[48] The strongest vibration mode of **1** was predicted to be 1756 cm^{-1} calculated at the ωB97X-D/aug-cc-pVTZ level of theory,[49] which matches well with the experimental result (1733 cm^{-1}).[46,47] Because FTIR absorptions can be

broadened due to the ice matrix, the measured absorptions of **1** and **18** overlap with the absorptions of acetaldehyde such as 2830 ($2\nu_6$), 1768 ($2\nu_9$), 1685 (ν_4 of $CH_3{}^{13}CHO$), 1389 (ν_6), and 885 (ν_{14} + ν_{15}) cm^{-1}. Since the absorption features of newly formed complex organics overlap, FTIR spectra alone cannot uniquely identify individual complex molecules such as **1** and its isomers, highlighting the need for an alternative, isomer selective technique to identify *individual* reaction products.[21,50]

Mass spectrometry

Isomer-selective photoionization reflectron time-of-flight mass spectrometry (PI-ReToF-MS)[21] was utilized here to identify **1** and **18**, as well as their enol tautomers **16**, 2-hydroxypropenal ($CH_2C(OH)CHO$, **19**), and 3-hydroxypropenal ($CH_3C(OH)CO$, **20**) based on their mass-to-charge ratios (*m/z*) and adiabatic ionization energies (IEs). Distinct experiments were conducted at photon energies of 11.10 eV, 9.87 eV, 9.39 eV, 8.77 eV, and 7.60 eV (Fig. 2). In low-temperature ices exposed to energetic electrons, radicals formed via hydrogen atom elimination recombine to form complex organic molecules. This has been well documented previously in irradiated carbon monoxide-containing ices[28,51,52] and acetaldehyde-containing ices.[18,50,53,54] Given this formation mechanisms for $C_3H_4O_2$ isomers in irradiated CO–CH_3CHO ices, **1** and **18** are first-generation products (Fig. 2). Tautomerization of **1** and **18** may lead to the formation of enols **16**, **19**, and **20** with high dose irradiation. To minimize sequential reactions, *low dose* irradiation experiments were performed. The PI-ReToF mass spectra of the *low dose* irradiated carbon monoxide–acetaldehyde ices recorded during TPD are shown in Fig. 4a. Focusing on the $C_3H_4O_2$ isomers, the TPD profile of the ion signal at *m/z* = 72 recorded at 11.10 eV (black line, Fig. 4b) shows an early sublimation event peaking at 249 K (Peak I) and a weak sublimation event peaking at 313 K (Peak II). A blank experiment was conducted for the CO–CH_3CHO ice without irradiation under otherwise identical conditions; no sublimation at *m/z* = 72 was observed (gray line, Fig. 4b), confirming that both peak I and II were caused by the irradiation exposure of the ices. The ion signal of *m/z* = 72 can be linked to the molecular formulae C_6, C_2O_3, $C_3H_4O_2$, C_4H_8O, and C_5H_{12}; therefore, it is imperative to use isotopically labeled precursors to assign the molecular formula(e). Substitution of CH_3CHO with CD_3CDO leads to products with four D atoms, which can be observed at *m/z* = 76 ($C_3D_4O_2^+$) in the CO–CD_3CDO ice (purple line, Fig. 4b); this finding confirms the presence of four hydrogen atoms. Replacing the CO–CH_3CHO ice with $C^{18}O$–

CH_3CHO ice shifts *m/z* by 2 atomic mass unit (amu) from *m/z* = 72 to *m/z* = 74, indicating the presence of one oxygen atom. Therefore, the ion signal at *m/z* = 72 can be linked to a molecule with the formula $C_3H_4O_2$.

At 11.10 eV, all five isomers **1** (IE = 9.29–9.60 eV), **16** (IE = 8.09–8.17 eV), **18** (IE = 10.00–10.21 eV), **19** (IE = 9.45–9.78 eV), and **20** (IE = 9.40–9.79 eV) can be ionized (Fig. 2, Tables S14–S15). Upon reduction of the photon energy to 9.87 eV, at which **18** (IE = 10.00–10.21 eV) cannot be ionized, Peaks I and II remain (Fig. 4c and Fig. S7); hence, there is no evidence for the detection of **18**. Due to the overlap of the IEs for isomers **1a** (IE = 9.52–9.60 eV), **19** (IE = 9.45–9.78 eV), and **20** (IE = 9.40–9.79 eV), it is difficult to distinguish these isomers using PI-ReToF-MS. It is worth noting that future experiments will aim to distinguish enols **19** and **20** using isomer-specific spectroscopic techniques such as photolysis[55,56] and photoionization efficiency (PIE) measurements. Here, the photon energy was then reduced to 9.39 eV, where only isomers **1b** (IE = 9.29–9.37 eV) and **16** (IE = 8.09–8.17 eV) can be ionized. At 9.39 eV, both peaks are still present (Fig. 4d), suggesting that Peaks I and II can be attributed to **1b** and/or **16**. It is worth noting that Peaks I and II are likely due to the cosublimation of compounds with the trimer ($C_6H_{12}O_3$, *m/z* = 132) and/or tetramer ($C_8H_{16}O_4$, *m/z* = 176) of acetaldehyde formed after irradiation (Fig. S8). In addition, three C_4H_8O isomers including 2-butanone ($CH_3CH_2C(O)CH_3$, IE = 9.45–9.53 eV),[57] butanal ($CH_3CH_2CH_2CHO$, IE = 9.75–9.83 eV),[57] and 2-methylpropanal ($(CH_3)_2CHCHO$, IE = 9.66–9.70 eV)[57] may contribute to Peaks I and II (Fig. S9); however, they cannot be ionized at 9.39 eV. Further lowering the photon energy to 8.77 eV, at which **1b** cannot be ionized, eliminates both peaks (Fig. 4d), indicating that Peaks I and II detected at 9.39 eV can be assigned to **1b**.

To further investigate the formation of enol **16**, additional *high dose* experiments were performed to induce keto-enol tautomerization pathways; the corresponding PI-ReToF mass spectra are compiled in Fig. 5a. At 8.77 eV, the TPD profile of *m/z* = 72 in the *high dose* irradiated CO–CH_3CHO ice reveals a weak sublimation event peaking at 207 K (Fig. 5b). Recall that no sublimation event was detected at 8.77 eV in the low dose experiment, so it is necessary to verify the molecular formula for this ion signal. The replacement of the CO–CH_3CHO ice by CO–CD_3CDO ice shifts the *m/z* by 4 amu from *m/z* = 72 to *m/z* = 76 (Fig. 5c), indicating once again the presence of four hydrogen atoms. Therefore, the ion signal at *m/z* = 72 can be clearly assigned to $C_3H_4O_2$ isomers. Note that other possible $C_3H_4O_2$ isomers such as 2-propenoic acid

($CH_2CHCOOH$, IE = 10.57 eV)[58] and propiolactone (*c*-CH_2CH_2COO, IE = 9.66–9.68 eV)[59] may form under *high dose* irradiation conditions; however, they cannot be ionized at 8.87 eV. Since only **16** (IE = 8.09–8.17 eV) can be ionized at 8.77 eV, this sublimation event peaking at 207 K must be linked to enol **16**. Upon reducing the photon energy to 7.60 eV, at which **16** cannot be ionized, no sublimation event was observed (Fig. 5d), confirming the formation of **16**. Overall, the low dose irradiation studies revealed the formation of isomer **1b**, whereas the high dose experiments further revealed the formation of the enol form **16**.

Having provided compelling evidence for the preparation of **1** and **16**, we now focus on their potential formation mechanisms. *First*, the unimolecular decomposition of acetaldehyde (**15**) upon exposure to the GCR proxies can lead to the formation of a hydrogen atom (Ḣ) and an acetyl radical **14** ($CH_3\dot{C}O$) via reaction (1). This reaction is endoergic by 368.1 ± 0.4 kJ mol^{-1},[60] which can be compensated for by an energy transfer from the impinging energetic electrons to **15**.[23] The formation of **14** was confirmed by FTIR spectroscopy in processed acetaldehyde ices using 5 keV electrons[37,53] and 0.8 MeV protons,[61] and the electron-irradiated acetaldehyde containing ice mixtures such as CO_2–CH_3CHO ice,[18] D_2O–CH_3CHO ice,[36] CH_4–CH_3CHO ice,[62] NH_3–CH_3CHO ice,[54] CH_3OH–CH_3CHO ice.[50,63] The suprathermal hydrogen atoms formed via reaction (1) have excess kinetic energies of a few eV.[64] They can add to carbon monoxide (**11**) to form the formyl radical **13** (HĊO) through reaction (2), which is exoergic by 60.9 ± 0.1 kJ mol^{-1}.[60] Previous work by Bennett et al. revealed an entrance barrier of reaction (2) at the CCSD(T)/aug-cc-pVTZ//B3LYP/6-311G(d,p) level of theory to be 11.2 kJ mol^{-1}.[65] This barrier can be overcome by the excess kinetic energy of the hydrogen atoms. The formation of **13** via reaction (2) has been demonstrated in processed carbon monoxide-containing ice mixtures such as CO–H_2O ice,[28,43,66,67], CO–H_2S ice,[52] CO–CH_4 ice,[68] and CO–CH_3OH ice.[69] Both radicals **13** and **14** were identified in our experiments by FTIR absorptions at 1852 cm^{-1} for **13** (HĊO, ν_3) and 1841 cm^{-1} for **14** ($CH_3\dot{C}O$, ν_3) in irradiated CO–CH_3CHO ices,[43-45] and at 1794 cm^{-1} for **13-**d_1 (DĊO, ν_3) and 1851 cm^{-1} for **14-**d_3 ($CD_3\dot{C}O$, ν_3) in irradiated CO–CD_3CDO ices (Fig. 3).[43,44] *Second*, **1** forms via a barrierless radical-radical recombination of **13** and **14** through reaction (3), which is exoergic by 308.9 ± 5.0 kJ mol^{-1}.[6,60] Recall that the TPD profile at *m/z* = 74 ($C_3H_4O^{18}O^+$) in $C^{18}O$–CH_3CHO ice overlaps the TPD profile at *m/z* = 72 ($C_3H_4O_2^+$) in CO–CH_3CHO ice, indicating that the formation of **1** involves one **11** and one **15** molecule.

[1] CH_3CHO (**15**) → $CH_3C\dot{O}$ (**14**) + $\dot{H}$ (+ 368.1 ± 0.4 kJ mol^{-1})[60]

[2] $\dot{H}$ + CO (**11**) → $H\dot{C}O$ (**13**) (– 60.9 ± 0.1 kJ mol^{-1})[60]

[3] $H\dot{C}O$ (**13**) + $CH_3C\dot{O}$ (**14**) → $CH_3C(O)CHO$ (**1**) (– 308.9 ± 5.0 kJ mol^{-1})[6,60]

Third, tautomerization of **1** leads to enol **16**. We investigated the potential energy surface computationally using the CBS–QB3 composite approach (Fig. S10). Our calculations did not find a transition state that connects **1** and **16**. Instead, **1** can first isomerize to enol **19** via keto-enol tautomerization (reaction (4)) with a barrier of 289.6 ± 8.0 kJ mol^{-1}, which is in good agreement with previous results (281 kJ mol^{-1}) calculated at the M06-2X/AVTZ level of theory.[6] The tautomerization of **19** then leads to **16** (reaction (5)) with a reaction barrier of 294.5 ± 8.0 kJ mol^{-1}.

[4] $CH_3C(O)CHO$ (**1**) ⇋ $CH_2C(OH)CHO$ (**19**) (+ 38.9 ± 8.0 kJ mol^{-1})

[5] $CH_2C(OH)CHO$ (**19**) ⇋ $CH_3C(OH)CO$ (**16**) (+ 46.8 ± 8.0 kJ mol^{-1})

Conclusions

This work presents the first bottom-up formation pathways of biorelevant methylglyoxal (**1**) — the simplest ketoaldehyde — and its enol tautomer 2-hydroxypropenone (**16**) in interstellar ice analogs. The low-temperature (5 K) ice mixtures of carbon monoxide (**11**) and acetaldehyde (**15**) were exposed to energetic electrons, simulating secondary electrons generated in the track of GCRs in cold molecular clouds with an age of (6 ± 2) × 10^6 years.[39] The formation of **1** was achieved through the barrierless recombination of the formyl (**13**) radical with the acetyl (**14**) radical. The overall reaction energy for the formation of **1** from **11** and **15** is endoergic by 8.3 ± 5.0 kJ mol^{-1}.[6,60] The isomer **16** was formed via the tautomerization process of **1**. Considering the distance of 2.0 ± 0.5 mm between the photoionization region and the ice surface[63] and the one dimensional average molecular velocity of 123 m s^{-1} for the sublimation of **16** from the surface at an average temperature of 207 K, the lifetime of the neutral **16** in the gas phase has to exceed 16.3 ± 4.1 μs. The observation of **1** and **16** provides the first experimental evidence for the tautomerization of ketoaldehydes in interstellar ice analogs composed of simple and abundant precursors. These results represent crucial steps toward a systematic understanding of how ketoaldehydes and their enol tautomers can be synthesized in interstellar ices.

Utilizing photoionization reflectron time-of-flight mass spectrometry (PI-ReToF-MS) and isotopic labeling studies, **1** and **16** were identified in the gas phase during TPD, suggesting their

formation in interstellar ices containing **11** and **15**. In interstellar ices, **11** has been detected at fractions of up to 55% with respect to water,[29] and **15** has been tentatively detected at levels of up to a few percent with respect to water.[30] Therefore, the presence of the hitherto astronomically unobserved **1** and **16** in the ISM is plausible. Due to their large dipole moments (5.03 D for **1b**, 2.83 D for **16**), they are promising candidates for future astronomical searches in star-forming regions using telescopes such as the Atacama Large Millimeter/submillimeter Array (ALMA). Once **1** forms within interstellar ices in a molecular cloud, it can serve as a precursor for sugars, sugar acids, and amino acids in deep space (Fig. 1). These molecules can be incorporated into accreting planetoids, asteroids, and comets,[70] and ultimately delivered to planets including early Earth, where they serve as an exogenous source for crucial biomolecules necessary for the *Origins of Life*.[18,71]

Supporting Information

Infrared spectra of carbon monoxide–acetaldehyde ices before and after irradiation (Figs. S1-S5), temporal evolution of radicals formed in high dose irradiated CO–CD_3CDO ice (Fig. S6), TPD profiles of *m/z* = 72 in CO–CH_3CHO ice recorded at 11.10 eV and 9.87 eV (Fig. S7), TPD profiles of $C_6H_{12}O_3$ and $C_8H_{16}O_4$ isomers recorded at 11.10 eV (Fig. S8), TPD profiles of C_4H_8O isomers recorded at 11.10 eV (Fig. S9), potential energy surfaces of isomerization of methylglyoxal (Fig. S10), experimental conditions (Table S1), VUV light generation parameters (Table S2), Cartesian coordinates, harmonic frequencies, infrared intensities, dipole moments of calculated structures (Tables S3-S8), detailed assignments of FTIR spectra (Tables S9-S13), error analysis of the adiabatic ionization energies and relative energies of isomers **1**, **16**, and **18-20** (Tables S14-S15), and the source code of the program for conformer sorting.

Author contributions

R. I. K. designed the experiments; J. W. and J. H. M carried out the experiments; J. W. conducted the data analyses; E. A. B, S. O. T., I. O. A. conducted the theoretical analysis; J. W., I. O. A., and R. I. K. wrote the manuscript, which was read, revised, and approved by all authors.

Competing interests

The authors declare no conflict of interest.

Acknowledgments

This work was funded by the US National Science Foundation, Division of Astronomical Sciences, under grant AST-2103269 (R. I. K.). The W. M. Keck Foundation and the University of Hawaii at Manoa funded the construction of the experimental setup.

Data availability

Essential data are provided in the main text and the Supporting Information. Additional data are available from the corresponding author upon reasonable request.

References

1. H. v. Pechmann, *Ber. Dtsch. Chem. Ges.*, 1887, **20**, 3213-3214.
2. R. T. Garrod, S. L. W. Weaver and E. Herbst, *Astrophys. J.*, 2008, **682**, 283.
3. P. de Marcellus, C. Meinert, I. Myrgorodska, L. Nahon, T. Buhse, L. L. S. d'Hendecourt and U. J. Meierhenrich, *Proc. Natl. Acad. Sci. U.S.A.*, 2015, **112**, 965-970.
4. E. Aguilar-Ovando, J. Cruz-Castañeda, T. Buhse, C. Fuentes-Carreón, S. Ramos-Bernal, A. Heredia and A. Negrón-Mendoza, *J. Radioanal. Nucl. Chem.*, 2018, **316**, 971-979.
5. J. Koucký, L. Kolesniková, K. Luková, K. Vávra, P. Kania, A. Coutens, J.-C. Loison, J. K. Jørgensen, A. Belloche and Š. Urban, *Astron. Astrophys.*, 2022, **666**, A158.
6. A. Coutens, J.-C. Loison, A. Boulanger, E. Caux, H. S. P. Müller, V. Wakelam, S. Manigand and J. K. Jørgensen, *Astron. Astrophys.*, 2022, **660**, L6.
7. A. Danchin and P. I. Nikel, *J. Mol. Evol.*, 2019, **87**, 271-288.
8. M. P. Kalapos, *J. Mol. Evol.*, 2021, **89**, 618-638.
9. Y. Wang and C.-T. Ho, *Chem. Soc. Rev.*, 2012, **41**, 4140-4149.
10. S. Bteich, M. Goubet, R. A. Motiyenko, L. Margulès and T. R. Huet, *J. Mol. Spectrosc.*, 2018, **348**, 124-129.
11. Miklós Péter Kalapos, *Drug Metabol. Drug Interact.*, 2008, **23**, 69-92.
12. S. Garai, B. Bhowal, M. Gupta, S. K. Sopory, S. L. Singla-Pareek, A. Pareek and C. Kaur, *Plant Sci.*, 2024, **338**, 111922.

13. S. Chakraborty, K. Karmakar and D. Chakravortty, *IUBMB Life*, 2014, **66**, 667-678.

14. R. A. Gomes, M. Sousa Silva, H. Vicente Miranda, A. E. N. Ferreira, C. A. A. Cordeiro and A. P. Freire, *FEBS J.*, 2005, **272**, 4521-4531.

15. Y. Inoue and A. Kimura, in *Advances in Microbial Physiology*, ed. R. K. Poole, Academic Press1995, vol. 37, pp. 177-227.

16. C. Gao, C. Ma and P. Xu, *Biotechnol. Adv.*, 2011, **29**, 930-939.

17. K. B. Muchowska, S. J. Varma and J. Moran, *Nature*, 2019, **569**, 104-107.

18. N. F. Kleimeier, A. K. Eckhardt, P. R. Schreiner and R. I. Kaiser, *Chem*, 2020, **6**, 3385-3395.

19. J. Wang, J. H. Marks, R. C. Fortenberry and R. I. Kaiser, *Sci. Adv.*, 2024, **10**, eadl3236.

20. C. Meinert, I. Myrgorodska, P. de Marcellus, T. Buhse, L. Nahon, S. V. Hoffmann, L. L. S. d'Hendecourt and U. J. Meierhenrich, *Science*, 2016, **352**, 208-212.

21. A. M. Turner and R. I. Kaiser, *Acc. Chem. Res.*, 2020, **53**, 2791-2805.

22. B. A. McGuire, *Astrophys. J., Suppl. Ser.*, 2022, **259**, 30.

23. R. Kaiser, G. Eich, A. Gabrysch and K. Roessler, *Astrophys. J.*, 1997, **484**, 487.

24. R. I. Kaiser, *Chem. Rev.*, 2002, **102**, 1309-1358.

25. C. J. Bennett, T. Hama, Y. S. Kim, M. Kawasaki and R. I. Kaiser, *Astrophys. J.*, 2011, **727**, 27.

26. B. C. Ferrari, K. Slavicinska and C. J. Bennett, *Acc. Chem. Res.*, 2021, **54**, 1067-1079.

27. P. Maksyutenko, R. Martín-Doménech, E. L. Piacentino, K. I. Öberg and M. Rajappan, *Astrophys. J.*, 2022, **940**, 113.

28. J. Wang, A. M. Turner, J. H. Marks, C. Zhang, N. F. Kleimeier, A. Bergantini, S. K. Singh, R. C. Fortenberry and R. I. Kaiser, *Astrophys. J.*, 2024, **967**, 79.

29. W.-F. Thi, E. F. van Dishoeck, E. Dartois, K. M. Pontoppidan, W. A. Schutte, P. Ehrenfreund, L. d'Hendecourt and H. J. Fraser, *Astron. Astrophys.*, 2006, **449**, 251-265.

30. E. L. Gibb, D. C. B. Whittet, A. C. A. Boogert and A. G. G. M. Tielens, *Astrophys. J., Suppl. Ser.*, 2004, **151**, 35-73.

31. V. M. Rivilla, L. Colzi, I. Jiménez-Serra, J. Martín-Pintado, A. Megías, M. Melosso, L. Bizzocchi, Á. López-Gallifa, A. Martínez-Henares, S. Massalkhi, B. Tercero, P. de Vicente, J.-C. Guillemin, J. García de la Concepción, F. Rico-Villas, S. Zeng, S. Martín, M. A. Requena-Torres, F. Tonolo, S. Alessandrini, L. Dore, V. Barone and C. Puzzarini, *Astrophys. J. Lett.*, 2022, **929**, L11.

32. B. M. Jones and R. I. Kaiser, *J. Phys. Chem. Lett.*, 2013, **4**, 1965-1971.

33. A. M. Turner, M. J. Abplanalp, S. Y. Chen, Y. T. Chen, A. H. Chang and R. I. Kaiser, *Phys. Chem. Chem. Phys.*, 2015, **17**, 27281-27291.

34. M. Bouilloud, N. Fray, Y. Benilan, H. Cottin, M. C. Gazeau and A. Jolly, *Mon. Not. R. Astron. Soc.*, 2015, **451**, 2145-2160.

35. R. L. Hudson, M. J. Loeffler, R. F. Ferrante, P. A. Gerakines and F. M. Coleman, *Astrophys. J.*, 2020, **891**, 22.

36. N. F. Kleimeier, A. K. Eckhardt and R. I. Kaiser, *Astrophys. J.*, 2020, **901**, 84.

37. N. F. Kleimeier and R. I. Kaiser, *ChemPhysChem*, 2021, **22**, 1229-1236.

38. D. Drouin, A. R. Couture, D. Joly, X. Tastet, V. Aimez and R. Gauvin, *Scanning*, 2007, **29**, 92-101.

39. A. G. Yeghikyan, *Astrophysics*, 2011, **54**, 87-99.

40. G. W. T. M. J. Frisch, H. B. Schlegel, G. E. Scuseria, M. A. Robb, J. R. Cheeseman, G. Scalmani, V. Barone, G. A. Petersson, H. Nakatsuji, et al., 2009.

41. R. I. Reed and J. C. D. Brand, *Trans. Faraday Soc.*, 1958, **54**, 478-482.

42. J. S. Crighton and S. Bell, *J. Mol. Spectrosc.*, 1985, **112**, 285-303.

43. A. K. Eckhardt, A. Bergantini, S. K. Singh, P. R. Schreiner and R. I. Kaiser, *Angew. Chem. Int. Ed.*, 2019, **58**, 5663-5667.

44. M. E. Jacox, *Chem. Phys.*, 1982, **69**, 407-422.

45. R. L. Hudson, *Phys. Chem. Chem. Phys.*, 2018, **20**, 5389-5398.

46. H. Niki, P. D. Maker, C. M. Savage, L. P. Breitenbach and M. D. Hurley, *J. Phys. Chem.*, 1987, **91**, 941-946.

47. M. Green, G. Yarwood and H. Niki, *Int. J. Chem. Kinet.*, 1990, **22**, 689-699.

48. M. E. S. Mirghani, Y. B. C. Man, S. Jinap, B. S. Baharin and J. Bakar, *Phytochem. Anal.*, 2002, **13**, 195-201.

49. R. D. Johnson, *NIST Standard Reference Database Number 101, Release 22, May 2022*.

50. J. Wang, J. H. Marks, A. M. Turner, A. A. Nikolayev, V. Azyazov, A. M. Mebel and R. I. Kaiser, *Phys. Chem. Chem. Phys.*, 2023, **25**, 936-953.

51. N. F. Kleimeier, A. K. Eckhardt and R. I. Kaiser, *J. Am. Chem. Soc.*, 2021, **143**, 14009-14018.

52. J. Wang, J. H. Marks, L. B. Tuli, A. M. Mebel, V. N. Azyazov and R. I. Kaiser, *J. Phys. Chem. A*, 2022, **126**, 9699-9708.

53. N. F. Kleimeier, A. M. Turner, R. C. Fortenberry and R. I. Kaiser, *ChemPhysChem*, 2020, **21**, 1531-1540.

54. J. H. Marks, J. Wang, N. F. Kleimeier, A. M. Turner, A. K. Eckhardt and R. I. Kaiser, *Angew. Chem. Int. Ed.*, 2023, **62**, e202218645.

55. A. Mardyukov, F. Keul and P. R. Schreiner, *Angew. Chem. Int. Ed.*, 2021, **60**, 15313-15316.

56. A. Mardyukov, R. C. Wende and P. R. Schreiner, *ChemComm.*, 2023, **59**, 2596-2599.

57. P. J. Linstrom and W. G. Mallard, *NIST Chemistry webBook, NIST Standard Reference Database Number 69*, 2013.

58. A. Katrib and J. W. Rabalais, *J. Phys. Chem.*, 1973, **77**, 2358-2363.

59. K. Watanabe, T. Nakayama and J. Mottl, *J. Quant. Spectrosc. Radiat. Transfer*, 1962, **2**, 369-382.

60. B. Ruscic and H. Bross, *Active Thermochemical Tables (ATcT) values based on ver. 1.122r of the Thermochemical Network*, ATcT.anl.gov, 2021.

61. R. L. Hudson and R. F. Ferrante, *Mon. Not. R. Astron. Soc.*, 2019, **492**, 283-293.

62. S. K. Singh, N. Fabian Kleimeier, A. K. Eckhardt and R. I. Kaiser, *Astrophys. J.*, 2022, **941**, 103.

63. J. Wang, J. H. Marks, A. M. Turner, A. M. Mebel, A. K. Eckhardt and R. I. Kaiser, *Sci. Adv.*, 2023, **9**, eadg1134.

64. C. Zhu, A. Bergantini, S. K. Singh, M. J. Abplanalp and R. I. Kaiser, *Astrophys. J.*, 2021, **920**, 73.

65. C. J. Bennett, C. S. Jamieson, Y. Osamura and R. I. Kaiser, *Astrophys. J.*, 2005, **624**, 1097-1115.

66. A. L. F. de Barros, C. Mejía, E. Seperuelo Duarte, A. Domaracka, P. Boduch, H. Rothard and E. F. da Silveira, *Mon. Not. R. Astron. Soc.*, 2022, **511**, 2491-2504.

67. A. Jiménez-Escobar, Y. J. Chen, A. Ciaravella, C. H. Huang, G. Micela and C. Cecchi-Pestellini, *Astrophys. J.*, 2016, **820**, 25.

68. S. Maity, R. I. Kaiser and B. M. Jones, *Astrophys. J.*, 2014, **789**, 36.

69. S. Maity, R. I. Kaiser and B. M. Jones, *Phys. Chem. Chem. Phys.*, 2015, **17**, 3081-3114.

70. Y. Furukawa, Y. Chikaraishi, N. Ohkouchi, N. O. Ogawa, D. P. Glavin, J. P. Dworkin, C. Abe and T. Nakamura, *Proc. Natl. Acad. Sci. U.S.A.*, 2019, **116**, 24440-24445.

71. D. P. Glavin, A. S. Burton, J. E. Elsila, J. C. Aponte and J. P. Dworkin, *Chem. Rev.*, 2020, **120**, 4660-4689.

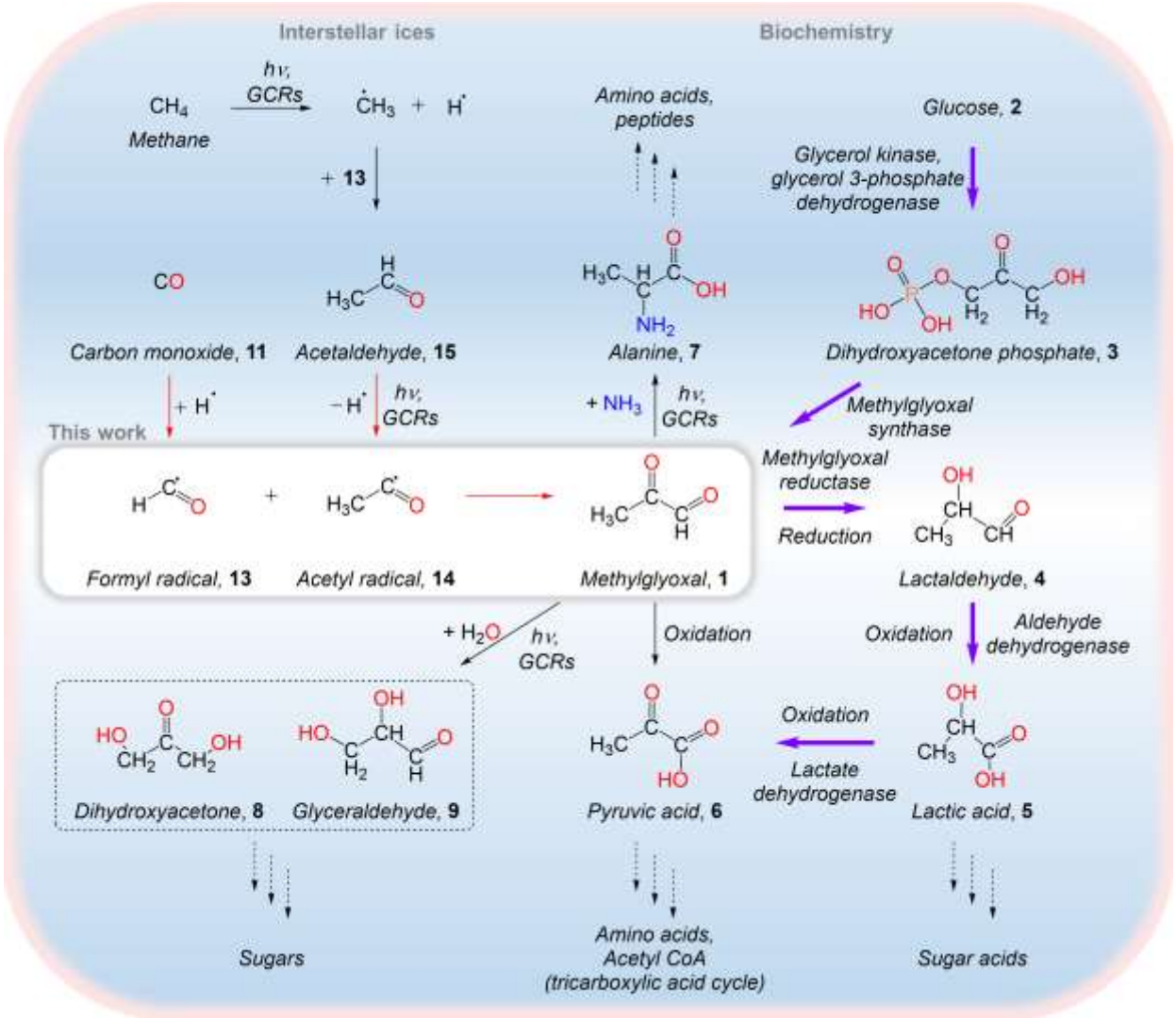

Fig. 1 Formation of methylglyoxal (**1**) in interstellar ices and its implications. The preparation of **1** is accomplished in low-temperature carbon monoxide–acetaldehyde (**11**−**15**) ice mixtures via energetic processing by galactic cosmic ray proxies. This reaction pathway involves carbon-carbon bond coupling through barrierless recombination of the formyl (HĊO, **13**) radical with the acetyl ($CH_3\dot{C}O$, **14**) radical. **1** serves as a precursor for critical biomolecules including lactaldehyde (**4**), lactic acid (**5**), pyruvic acid (**6**), the proteinogenic amino acid alanine (**7**), and the simplest sugar molecule glyceraldehyde (**9**). In contemporary biochemistry, **1** plays a central role in the methylglyoxal pathway (purple arrows) that converts glucose (**2**) into pyruvate, linking to the tricarboxylic acid (TCA) cycle.

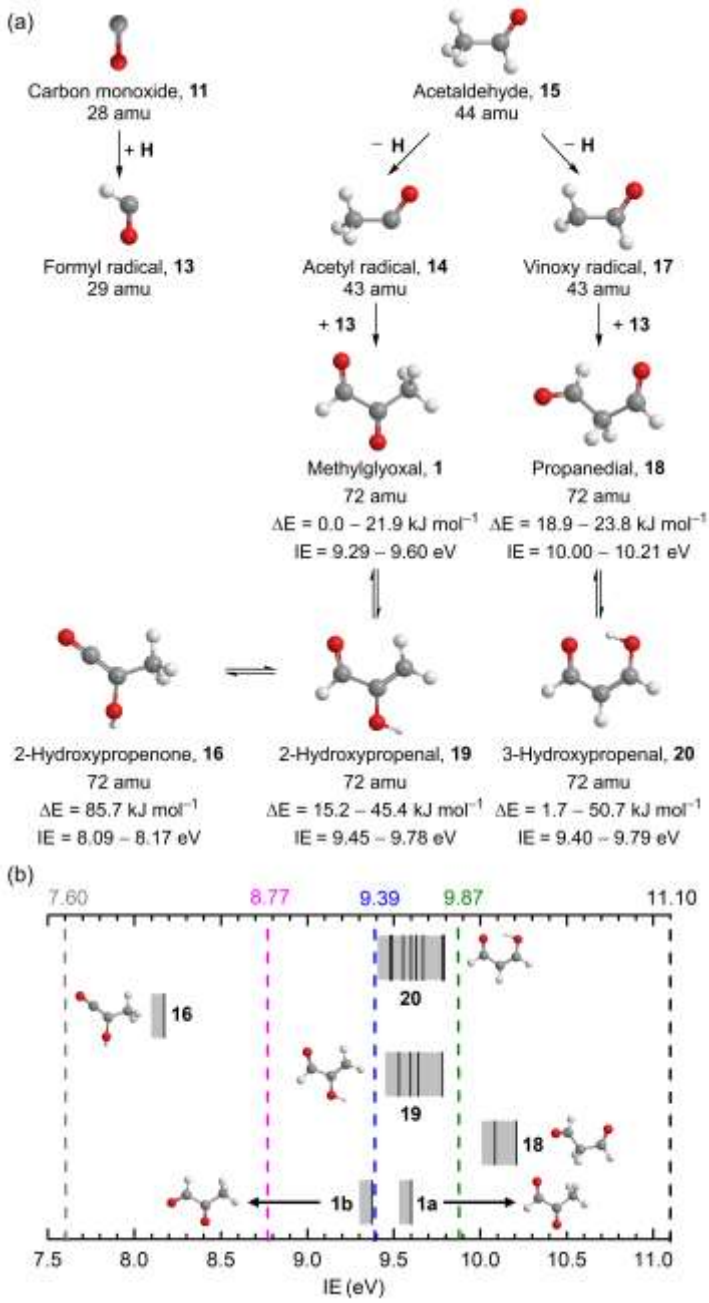

Fig. 2 Reaction scheme leading to isomers **1**, **16**, and **18-20** in irradiated carbon monoxide–acetaldehyde ices (a). Barrierless radical-radical reactions **13** plus **14** and **13** plus **17** produce **1** and **18**, respectively; tautomerization of **1** and **18** may lead to enols **16**, **19** and **20**. The IEs are computed at the CBS–QB3 level of theory and are corrected by incorporating error (Tables S6-S7). The bottom figure compiles the calculated IEs of isomers (black solid line) and ranges of the conformers (grey area) after error analysis (b). VUV photon energies (dashed lines) were selected to photoionize subliming molecules in the gas phase during TPD.

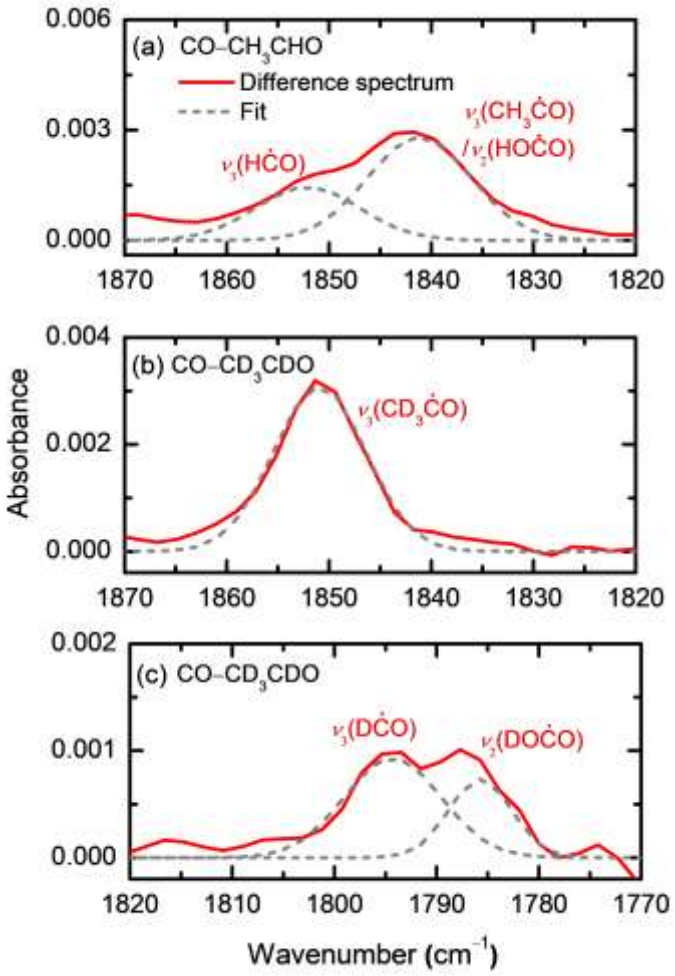

Fig. 3 Difference infrared spectra between the irradiated and pristine carbon monoxide–acetaldehyde ices at 5 K. The new observed infrared absorptions in high dose irradiated CO–CH_3CHO ice (a) and CO–CD_3CDO ice (b and c) can be assigned to the formyl (**13**), acetyl (**14**), and hydroxycarbonyl radicals.

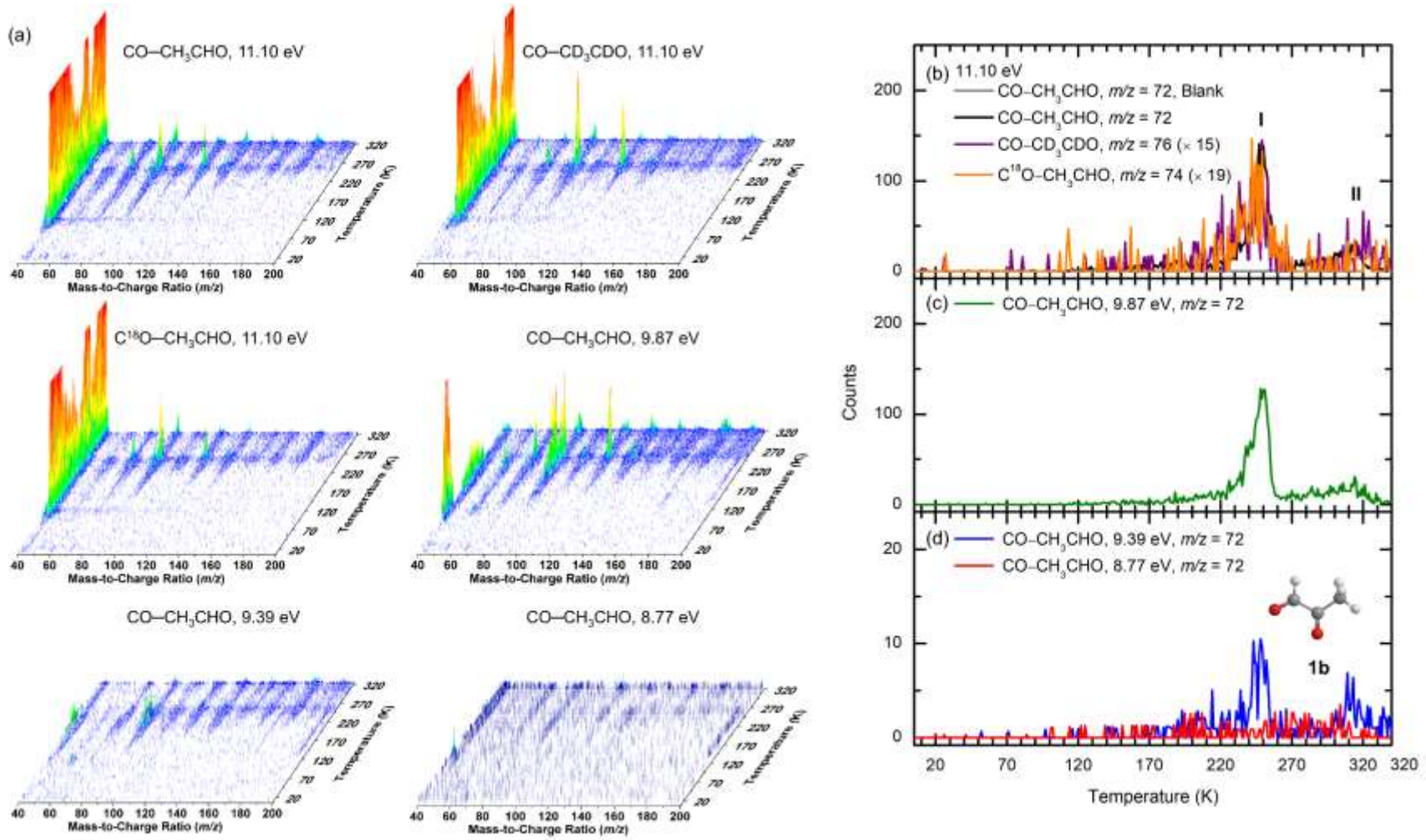

Fig. 4 PI-ReToF-MS data during TPD of carbon monoxide–acetaldehyde ices with low dose irradiation. Data were recorded for the irradiated CO–CH_3CHO ice at 11.10 eV, 9.87 eV, 9.39 eV, and 8.77 eV, the irradiated CO–CD_3CDO ice at 11.10 eV, and the irradiated $C^{18}O$– CH_3CHO ice at 11.10 eV (a). TPD profiles of *m/z* = 72 in CO–CH_3CHO ice were recorded at 11.10 eV (b), 9.87 eV (c), 9.39 eV and 8.77 eV (d).

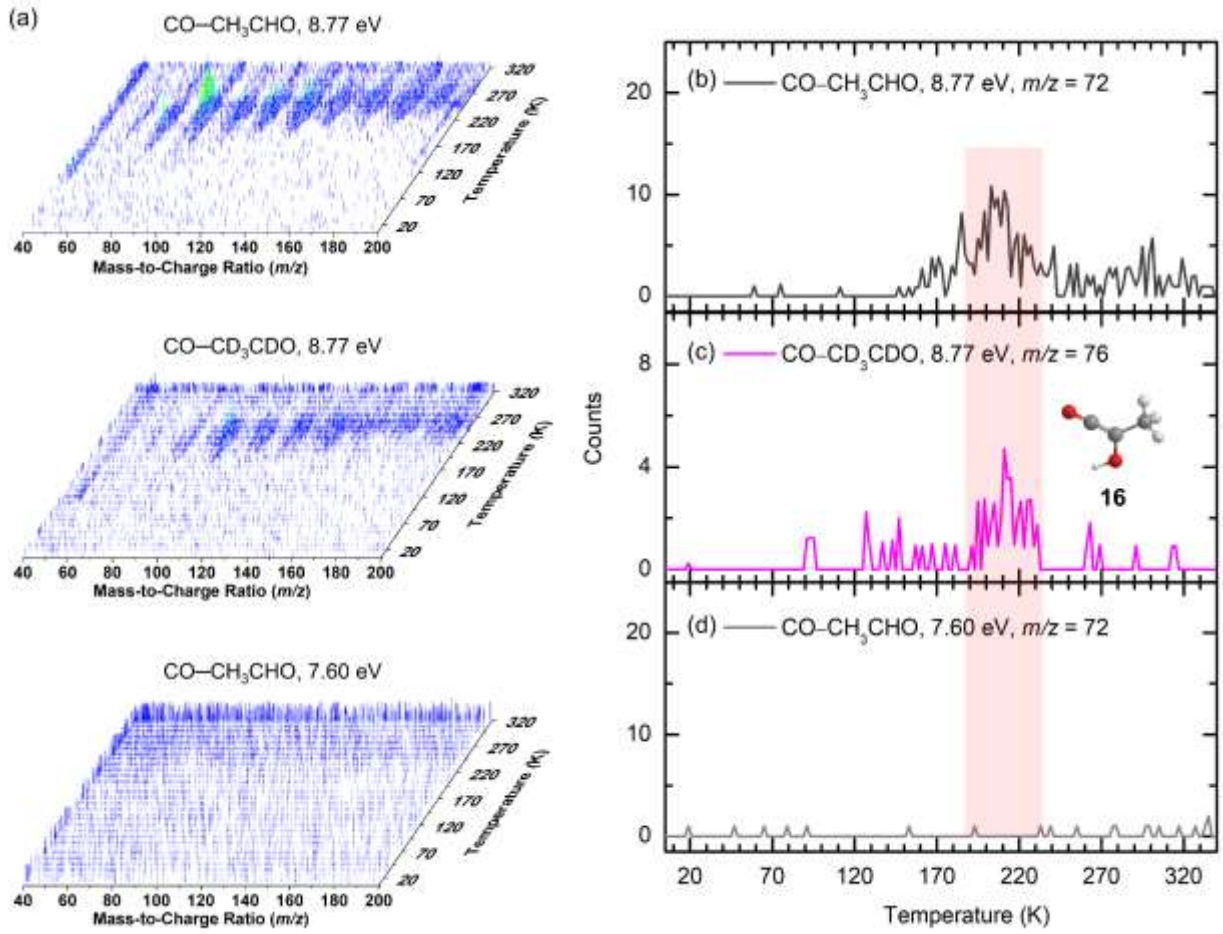

Fig. 5 PI-ReToF-MS data during the TPD of carbon monoxide–acetaldehyde ices with high dose irradiation. Data were recorded for the irradiated CO–CH_3CHO ice at 8.77 eV and 7.60 eV, and the irradiated CO–CD_3CD_2OD ice at 8.77 eV (a). TPD profiles of *m/z* = 72 in irradiated CO–CH_3CHO ice were measured at 8.77 eV (b) and 7.60 eV (d). TPD profile of *m/z* = 76 in irradiated CO–CD_3CD_2OD ice was recorded at 8.77 eV (c). The red shaded region indicates the sublimation region corresponding to enol **16**.

Data availability

Essential data are provided in the main text and the Supporting Information. Additional data are available from the corresponding author upon reasonable request.